

**MSEC2010-34271**

## **FEMTOSECOND LASER-INDUCED SURFACE TEXTURING AND CRYSTALLIZATION OF A-SI:H THIN FILM**

**Hongliang Wang, Panjawat Kongsuwan, Gen Satoh, Y. Lawrence Yao**

Department of Mechanical Engineering  
New York, NY, USA

### **ABSTRACT**

Hydrogenated amorphous silicon (a-Si:H) thin films have been considered for use in solar cell applications because of their significantly reduced cost, however, the overall efficiency and stability are less than that of their bulk crystalline counterparts. Limited work has been performed on solving the efficiency and stability issues of a-Si:H simultaneously. In this study, both surface texturing and crystallization on a-Si:H thin film are achieved through one-step femtosecond laser processing in water. Light absorption is enhanced by light trapping based on surface geometry changes, and the formation of a mixture of hydrogenated microcrystalline silicon ( $\mu\text{-Si:H}$ ) and a-Si:H after crystallization suggests that the overall stability may be increased. Furthermore, the formation mechanism for the surface spikes is discussed. A comparison of absorptance spectra for various surface morphologies and crystallinities shows that the combination of surface texturing and crystallization induced by femtosecond laser processing is very promising for a-Si:H thin film solar cell applications.

### **INTRODUCTION**

Many industrial solar cells in use today use bulk materials as absorbers with crystalline silicon being the most prevalent. However, crystalline silicon suffers from the disadvantage of high material cost primarily due to its low absorption coefficient. Recently, thin film absorbers are becoming more and more attractive based on their potential for low-cost modules, possibility to create tandem junctions and large-scale manufacturing [1-3]. a-Si:H is the most popular material for use in thin film form due to its low energy economy (watt/cost). The main issue with a-Si:H is the high order of dangling bonds which act as recombination centers that severely reduce the carrier lifetime and make the efficiency as low as around 10%. Additionally, this initial efficiency will decrease by 50% or more when exposed to sunlight over a period of months which is known as the Staebler-Wronski effect or SWE [4-6].

Due to their instability and low efficiency, a thin-film a-Si:H solar cell requires a highly efficient light-trapping design to absorb a significant fraction of the incident sunlight and

material property changes to increase stability. Antireflection coatings and front-side texturing through the use of alkaline-based solution, such as KOH and NaOH, etching and high energy ion beam or pulsed laser irradiation have been used to enhance light trapping [7-10]. Although the absorptance is increased, the SWE still remains due to the high disorder in the a-Si:H network which causes atoms to have dangling bonds [5-6]. In order to reduce the SWE, hybrid a-Si/ $\mu\text{-Si}$  tandem modules have been developed and are able to achieve both higher efficiency and stability compared with single junction a-Si:H [11], due to the use of a thinner a-Si layer and the wider spectral absorption of  $\mu\text{-Si}$ . To eliminate the need for two deposition steps, laser-induced crystallization of a-Si:H has been proposed to produce a mixture of  $\mu\text{-Si:H}$  and a-Si:H and simultaneously form a light trapping texture on the surface of the material. Therefore, laser-based treatment of a-Si:H may solve its efficiency and stability issues in a one-step process, which is a promising methodology for thin-film solar cell fabrication.

While both nanosecond and femtosecond pulsed lasers are useful tools for a-Si:H crystallization [12-13], the femtosecond laser-induced crystallization includes a non-thermal ultrafast phase transition and followed by a thermal effect process which is different from rapid thermal melting and resolidification caused by a nanosecond laser [14]. Surface texturing can also be achieved by both femtosecond and long-pulse lasers, however, femtosecond lasers are better suited for precise micromachining due to their extremely high peak power and ultrashort pulse duration, which leads to greatly reduced thermal energy diffusion and heat-affected-zone [15-16]. Therefore, for texturing on a limited thickness of thin films, femtosecond laser is more desirable. A number of different techniques have been reported for forming microstructures on silicon surfaces using femtosecond lasers. Mazur, et al. [17-19] showed micron-size conical spikes on crystalline silicon when irradiated with hundreds of femtosecond laser pulses in different background gases, such as SF<sub>6</sub>, N<sub>2</sub>, and air, and pointed out a significant enhancement in light absorptance after texturing. Formation of submicron spikes and nano-period

ripples on crystalline silicon has also been investigated after femtosecond laser irradiation in water, and produces much denser spikes than when processed in a gas environment [20-21]. Compared to the successful light trapping enhancement on bulk crystalline silicon, limited work is focused on a-Si:H thin films. Nayak, et al. [22] reported the observation of crystallization and simultaneous formation of surface microstructures in a-Si:H thin films through femtosecond laser processing in air, and showed that the nano-sizes spikes resulted in strong light absorption. However, the light trapping geometry for a-Si:H surfaces has not been estimated for different processing environments, such as in other background gases or water.

In this paper, the formation of a densely packed, spiked surface structure has been studied through scanning electron microscopy and atomic force microscopy for femtosecond laser irradiation of a-Si:H thin films in water, and light absorptance dependence of surface structure is studied by spectrophotometry. The effect of laser processing on crystallinity is investigated by x-ray diffractometry (XRD). The combined effects of light trapping surface structure and crystallization in a-Si:H shows a one-step process for potentially enhancing the efficiency and stability of thin film solar cells.

## BACKGROUND

### Laser interaction with wide-band gap material

Femtosecond lasers are able to interact with materials that have higher band gaps than the laser photon energy due to their ultrashort and high intensity pulses. In the case where the intensity of the femtosecond laser pulse reaches  $10^{13} - 10^{15}$  W/cm<sup>2</sup> or more, multiphoton or tunneling ionization will occur within a few to tens of femtoseconds. When the intensity drops below  $10^{12}$  W/cm<sup>2</sup>, avalanche (or collisional) ionization which is described by the Fokker-Planck equation occurs [16]:

$$\frac{\partial}{\partial E_K} \left[ R_j(E_K, t) N(E_K, t) - \alpha(E_K) E_p N(E_K, t) - D(E_K, t) \frac{\partial N(E_K, t)}{\partial E_K} \right] + \frac{\partial N(E_K, t)}{\partial t} = S(E_K, t) \quad (1)$$

where  $N$  is the electron density distribution,  $E_K$  is the electron kinetic energy,  $E_p$  is the phonon energy,  $t$  is the time,  $R_j$  is the heating rate of electrons,  $\alpha$  is the electron-phonon energy transfer to the material,  $D$  is the diffusion coefficient and  $S$  indicates sources and sinks of electrons. More details about avalanche ionization can be found in [16].

As the excited electron density increases, the material is first transformed into a plasma that reflects and absorbs the remaining pulse energy. After pulse duration, the energy absorbed by the electrons is transferred to the material over a picosecond time scale. Within a few microseconds, the thermal energy of the plasma that diffuses out from the focal volume can cause thermal melting or vaporization and can leave behind permanent structural damage for sufficiently high intensities [23-24]. Femtosecond laser also can induce “cold” ablation

caused by ion pulling out from the material if the electric field formed by the excited electrons is high enough. This critical electron density can be estimated by [16],

$$n_{cr} = \frac{\pi m_e c^2}{e^2 \lambda^2} \quad (2)$$

where  $m_e$  is the electron mass,  $c$  is the speed of light,  $e$  is the electron charge, and  $\lambda$  is the laser wavelength.

### Femtosecond laser-induced crystallization

During femtosecond laser irradiation, the conservation equation for electrons excited by multiphoton absorption can be estimated as [14],

$$\frac{\partial N(x, t)}{\partial t} = \frac{(1-R)\alpha I(x, t)}{h\nu} + \frac{(1-R)^2 \beta I^2(x, t)}{2h\nu} \quad (3)$$

where  $N$  is electron density,  $R$  is reflectivity,  $\alpha$  is linear absorption coefficient,  $h\nu$  is the energy of the laser beam,  $\beta$  is the two photon absorption coefficient, and  $I(x, t)$  is the laser intensity expressed as follows [14],

$$\frac{\partial I(x, t)}{\partial t} = -(\alpha + \Theta N)I \quad (4)$$

where  $\Theta$  is the free carrier absorption cross section.

If more than a critical density that is estimated to be  $10^{22}$  cm<sup>-3</sup> [14] of electrons, which are excited out of the bonding states of the valence band into the conduction band is achieved, then a non-thermally ultrafast phase transition will occur. Due to the removal of a significant number of electrons from the material, the bond charge will be so weak that the material structure will no longer be stable and it collapses caused by the atoms' enhanced mobility and the phase changes to fluid without thermal effect [25-26]. This ultrafast phase transition caused by high density photo-excited plasma without increasing the materials thermal energy is called the plasma annealing mechanism. Van Vechten, et al. [25] showed that, as the plasma becomes less dense due to expansion and energy transfer to the material, the material will pass back through the phase transition and covalent bonding will gradually reappear. Crystallization of the material can occur if this solidification process does not occur too quickly. Choi, et al. [14] considered that the non-thermally melted layer vanishes in a few picoseconds during which time a portion of the covalent bonds start reappearing due to relaxation of electrons back to the valence band. Within a nanosecond, the surface starts to be melted due to thermal diffusion after the transfer of energy from the excited electrons to the material. Resolidification of this thermal melting layer causes the final crystallization. Callan, et al. [27] also believes that the ultrafast phase transition described above does not lead to a thermodynamically stable crystalline phase, but to a nonequilibrium disordered phase, and this disorder-to-disorder phase transition can cause defect formation which is suggested as the driving force for subsequent rapid nucleation [14]. This process including non-thermal and thermal melting leading to solidification describes femtosecond laser-induced

crystallization, which is different from nanosecond laser crystallization via rapid melting and solidification process.

### Surface texturing mechanism in water

The periodic surface structure generated on silicon by femtosecond laser irradiation is produced through a different mechanism compared to the craters formed by conventional pulsed laser ablation. Mazur, et al. [17, 20] showed spike formation on crystalline silicon surfaces by femtosecond laser irradiation in both gas and water environments, and suggested two stages to explain the mechanisms. For a water environment, in the first stage, most of the light is absorbed by a silicon layer tens of nanometers thick near the silicon–water interface which creates a plasma. Due to the high temperature of the plasma, micro-size bubbles are generated by the decomposition of water. Diffraction of the laser beam by those bubbles produces ripple-like structures on the silicon surface due to the existence of high and low intensity fringes. The separation between adjacent rings is found to be close to the wavelength of the laser. Roughness on the silicon surface causes the laser pulse energy to be non-uniformly absorbed across the surface, which results a random arrangement of bubbles. The superposition of ripple structures generated by multiple laser pulses causes bead-like structures to be randomly distributed on the surface of the material. During the first stage of processing in a gas environment, straight wavelength-dependent ripple structures are first formed on the silicon surface due to light- induce periodic surface structure (LIPSS), then micron-scale ridges are generated on the top of and perpendicular to the ripples. The coarsened layer breaks up into micron-size beads that are suggested to be caused by surface tension effects [17]. The second stage of surface structure formation is similar for processing in both water and gas environments. The beads that formed in the first stage act to concentrate subsequent laser light into the valleys between them through reflection off the sides of the beads. This causes the ablation rate to be higher inside the valleys than on the bead tips, which leads to sharpening of the beads into spikes after hundreds of laser pulse assisted texturing steps. It is noted that, in water, the spikes are generated with submicron heights and wavelength-dependent spacing and are much shorter and denser than those formed in gas environments.

### EXPERIMENTAL SETUP

Amorphous silicon films were deposited on 0.525mm-thick Corning 1747 glass substrates using plasma enhanced chemical vapor deposition (PECVD). The a-Si:H film was deposited at a rate of 60 Å/s in an hydrogen diluted silane environment at 380°C, with a hydrogen atomic concentration of around 20 at %. Film thickness was found to be about 1.6 μm through ellipsometry measurements (Fig. 1).

Femtosecond laser experiments were carried out using a commercial Ti:sapphire oscillator and regenerative amplifier system. The system delivered 130-fs pulses of linearly polarized light at a 1 KHz repetition rate, and a central

wavelength of 800 nm. The a-Si:H films were cleaned with acetone in an ultrasonic cleaner for 5 minutes and then rinsed with methanol and distilled water prior to processing. The sample was placed in a plastic container that was mounted on a three-axis translation stage and irradiated by laser pulses focused by a 60 mm focal-length lens. The laser beam traveled through 5 mm of distilled water before striking the sample surface. The focal plane was placed below the sample surface to create a circular beam spot on the sample surface with a diameter of 150 μm. An area of 10×15 mm<sup>2</sup> was processed at the fluence of 0.5 J/cm<sup>2</sup> by scanning the sample under the stationary laser beam at a speed of 25 mm/s with a 50 μm spacing between lines for both X-ray diffraction (XRD) and spectrophotometer measurements. For the morphology study, it was more concerned on the effects of fluence and number of pulses. The stationary samples were irradiated at higher fluences (1 J/cm<sup>2</sup> to 1.8 J/cm<sup>2</sup>) in water with different numbers of pulses (2-100) at different spots with a spot diameter of 150 μm.

The untreated and treated samples were observed through scanning electron microscopy (SEM). Surface roughness and the distribution of spikes in the treated samples were also examined using an atomic force microscopy (AFM). The optical transmittance and reflectance of both untreated and treated samples were measured by a spectrophotometer over a wavelength range of 250 nm-2500 nm which corresponds to the main spectral range of solar irradiation [28]. The reflectance ( $R$  in %) and transmittance ( $T$  in %) are then used to calculate the absorptance ( $A$  in %) of the film:  $A=100-R-T$ . XRD (Cu K<sub>α</sub>-line) was used for crystallinity estimation.

### RESULTS AND DISCUSSION

The measured and fitted Psi ( $\Psi$ ) and Delta ( $\Delta$ ) curves from ellipsometer measurements of the as-received a-Si:H films are shown in Fig. 1. The thickness is determined to be 1578.6±2.28 nm with a surface roughness of 2.62±0.28 nm, the variation represents standard deviation. It is observed that the model generated data matches experimental data well for both number of oscillations and spectral locations.

Figure 2 shows the SEM and AFM images of the initial surface of the a-Si:H film. The surface appears smooth from SEM image, and the surface average roughness measured by AFM is 2.08 nm, which is close to that measured by the ellipsometer. Therefore, the surface is relatively flat of the as-received a-Si:H film.

### Absorptance spectra of as-received film

The light transmittance and reflectance of the a-Si:H thin film are measured by a spectrophotometer in the range of 250nm to 2500 nm, and absorptance is calculated based on the above two measurements. A numerical model to predict the absorptance spectrum of an a-Si:H film with planar interfaces to compare with the measurement. The model configuration consisting of an a-Si:H thin film on a glass substrate is shown in Fig. 3 where the refractive index of a-Si:H is  $n$ , its extinction

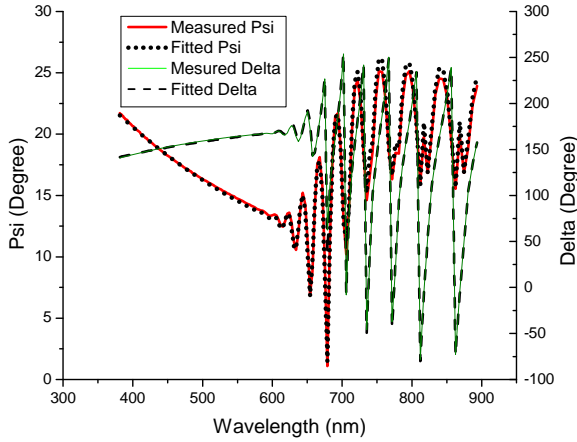


**Figure 1 Comparison of measured and model fitted optical data in the ellipsometer measurement of a-Si:H layer thickness that deposited on glass substrate**

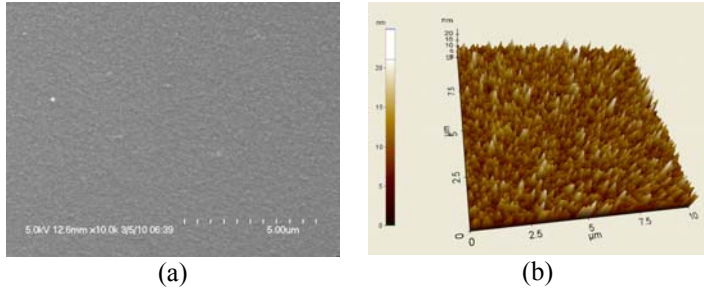


**Figure 2 (a) SEM image and (b) AFM image of as-received a-Si:H film surface, average roughness  $R_a$  is around 2nm as measured by AFM**

coefficient is  $k$ , and the film thickness is  $d$ . The glass substrate has a refractive index of  $s$  and absorption coefficient of zero, and the thickness of the substrate is several orders of magnitude larger than  $d$ . The surrounding air has an index of refraction,  $n_0$ , of one. Since the film thickness is much larger than the surface roughness, surface roughness is ignored in the model. This is further justified by the fact that internal interference induced oscillation is observed in the measured transmittance spectrum shown in Fig. 4, and it indicates the thickness of the film is uniform.

The transmittance through the film/substrate pair is estimated by considering the light reflection and refraction at the interface between different mediums and the absorption inside the a-Si:H film as below [29],

$$T = \frac{Ax}{B - Cx + Dx^2} \quad (5)$$

where,  $A = 16n(s^2 + k^2)$ ,  $B = [(n+1)^2 + k^2][(n+1)(n+s^2) + k^2]$ ,  $C = [(n^2 - 1 + k^2)(n^2 - s^2 + k^2) - 2k^2(s^2 + 1)]2\cos\varphi - k[2(n^2 - s^2 + k^2) - (s^2 + 1)(n^2 - 1 + k^2)]2\sin\varphi$ ,  $D = 2(n-1)^3(n-s^2)$ ,  $\varphi = 4\pi nd/\lambda$ , and  $x = e^{-4\pi k/\lambda}$ .

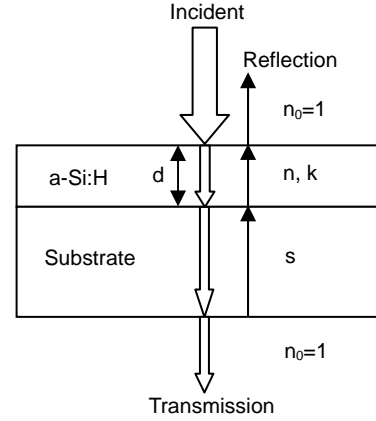


**Figure 3 Schematic of one-dimensional absorption simulation model of as-received a-Si:H film on glass substrate, film thickness  $d=1.6\mu\text{m}$ , real and imaginary parts of refractive index of a-Si:H film are  $n$  and  $k$ ,  $s$  and  $n_0$  are the refractive index of the substrate and air**

Among these parameters,  $s$  and  $d$  can be easily determined, and  $n$  and  $k$  are functions of wavelength, therefore,  $T=T(n, k)$ . Determination of the optical constants ( $n, k$ ) is the first step of the modeling. In this paper, we followed the method described by Swanepoel, et al. [29] and use the transmittance measurement to determine the optical constants from the interference fringes. The basic equation of interference is

$$2nd = m\lambda \quad (6)$$

where  $m$  is an integer for maximum and integer plus a half for minimum.

In Fig. 4, at the region where the photon energy is less than the band gap of a-Si (1.7eV or 730nm) and cannot be fully absorbed, the interference fringes of the model can be written as the maximum and minimum transmittance values for Eq. (5) for  $k=0$  [29] as,

$$T_{peak} = \frac{A'x}{B' - C'x + D'x^2} \quad T_{valley} = \frac{A'x}{B' + C'x + D'x^2} \quad (7)$$

where,  $A' = 16ns^2$ ,  $B' = (n+1)^3(n+s^2)$ ,  $C' = 2(n^2 - 1)(n^2 - s^2)$ , and  $D' = 2(n-1)^3(n-s^2)$

The optical constants can be calculated using Eq.(7) at the corresponding wavelengths that cause peaks and valleys, and a polynomial curve fitting of those values gives the optical constants in the required spectrum. The reflectance can be estimated by the correlation among the light reflection, transmission, a-Si:H absorption coefficient and film thickness [30],

$$\alpha = \frac{1}{d} \ln \left[ \frac{(1-R)^2 + \sqrt{(1-R)^4 + 4R^2T^2}}{2T} \right] \quad (8)$$

The simulation parameters used in the calculation are, substrate refractive index  $s=1.5$  and film thickness  $d=1600\text{nm}$ . As seen in Fig. 4, the transmittance simulation results show a good agreement with the measurement in both periodicity and magnitude. Reflectance curves for experimental and numerical

results in Fig. 5 show that the simulation has the same periodicity as the measurement, however, the simulation values are 10 to 15% lower than those measured experimentally. The under estimate could be caused by ignoring the interface between the glass substrate and air in the model. Based on the

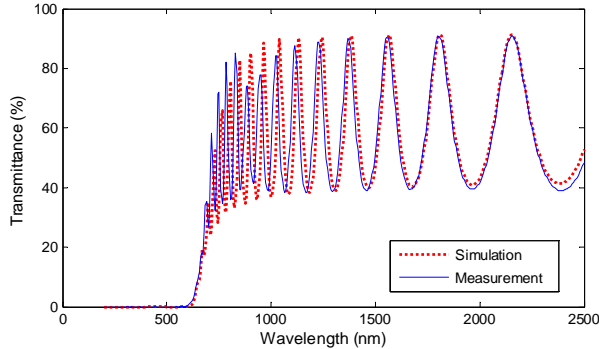


**Figure 4 Comparison of transmittance spectra for both simulation and measurement by spectrophotometry of as-received a-Si:H film on glass substrate, film thickness is 1.6µm**

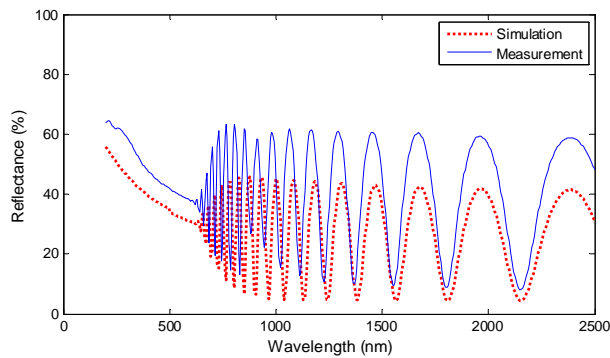


**Figure 5 Comparison of reflectance spectra for both simulation and measurement by spectrophotometry of as-received a-Si:H film on glass substrate, film thickness is 1.6µm**

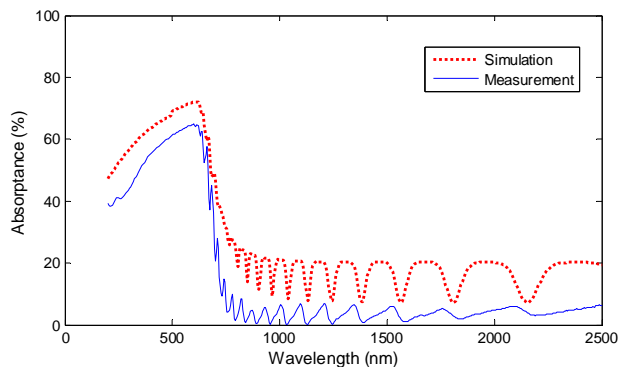
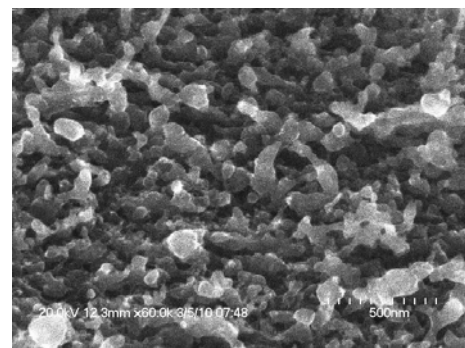


**Figure 6 Comparison of calculated absorptance spectra ( $A=100-T-R$ ) of as-received a-Si:H film on glass substrate based on both transmission and reflection simulation and measurement by spectrophotometry, film thickness is 1.6µm**

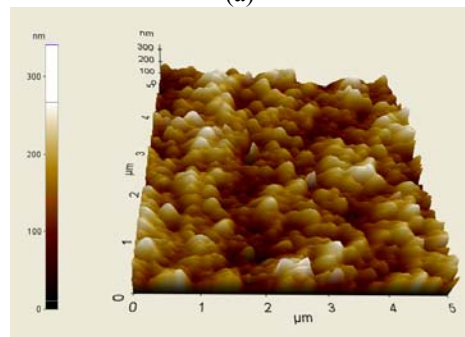
similar transmittance values and lower reflectances, the simulated absorptance ( $A=100-R-T$ ) is higher than measured experimentally as shown in Fig. 6, however the overall wavelength dependence is captured by the model.

### Effect of laser processing on absorptance and crystallinity

Figure 7 (a) is an SEM image of an a-Si:H film surface laser treated in water. The small nano-size spikes with blunt tips are randomly orientated and irregularly distributed on the surface after laser treatment. When observed optically, the surface of the processed a-Si:H film is much darker than the original shiny reddish gray color which shows that the textured surface has the capability of light trapping which greatly reduced the visible light reflection. The surface roughness and spike distribution is further observed in the AFM image in Fig. 7 (b), which shows an average spike height of  $138\pm 2.58$  nm and the average spike spacing of  $216\pm 6.77$  nm, the variation represents the standard error. The spacing determination methodology is described later.



(a)



(b)

**Figure 7 (a) SEM image and (b) AFM image of laser irradiated surface of a-Si:H film (fluence of  $0.5\text{J}/\text{cm}^2$ , scanning speed at  $25\text{mm}/\text{s}$ ), showing texturing with randomly oriented spikes on the surface**

These irregular spikes generated on the a-Si:H surface may be due to the low laser fluence and pulse overlap that cannot fully remove the material during processing. The plasma generated at the silicon-water interface and the scattering effects induced by the bubbles and suspended ablated material

will shield the target, therefore, part of the incident energy will be lost before reaching the material resulting in an ablation threshold for underwater treatment that is higher than that in air ( $\sim 0.2\text{J}/\text{cm}^2$ ) [31]. Moreover, decreasing the number of pulses can increase the ablation threshold, due to modification of the absorption behavior of the film such that subsequent damage occurs at fluence levels lower than for previous pulses [21]. Therefore, the experimental condition ( $0.5\text{ J}/\text{cm}^2$  at scan speed of  $25\text{ mm}/\text{s}$ ) is considered to be near the ablation threshold for laser processing in water, so that the majority of the material is melted rather than ablated. Resolidification of the melted silicon layer may cause the randomly distributed irregular spikes on the surface as well as the crystallization. This is different from crystalline silicon processing [17, 20] in which the well ordered spikes are generated by laser ablation.

Figure 8 shows the absorptance spectra for both the treated and untreated films and depicts a dramatic increase in the absorptance of the treated a-Si:H film over the entire spectrum. The absorptance goes up to more than 90% from UV wavelengths to the band gap of a-Si:H (730nm) due to multiple reflections caused by the surface texture, and decreases almost linearly below the band gap. For untreated a-Si:H, light at wavelengths larger than 730nm does not contain enough energy to promote an electron from the valence band to the conduction band so that the absorptance is close to zero. The non-zero below-band gap absorptance of treated a-Si:H could be attributed to crystallization (band gap of  $\mu\text{c-Si:H}$  is  $1.1\text{eV}$  or  $1100\text{nm}$ ) [32] which broadens the absorption range to  $1100\text{nm}$  while the textured surface introduces light trapping through multiple reflections. Moreover, the impurity and defect concentration induced during laser processing can cause several sub-band gaps to form which could absorb light with even longer wavelengths. The reason why the absorptance starts decreasing at  $730\text{nm}$  rather than staying constant to  $1100\text{nm}$  is due to the small amount of crystallized material and

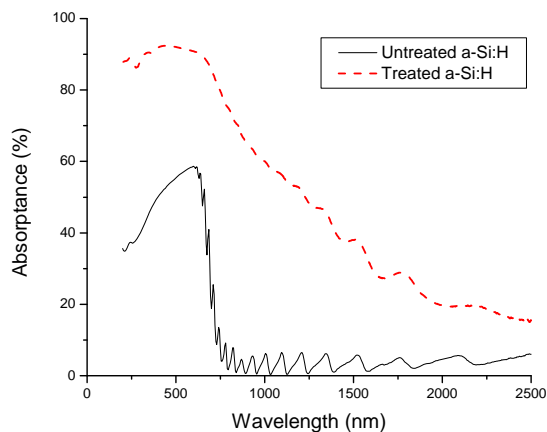


**Figure 8 Comparison of absorptance spectra measurement of as-received and laser treated a-Si:H film by spectrophotometry (fluence of  $0.5\text{J}/\text{cm}^2$ , scan at  $25\text{mm}/\text{s}$ ), showing increase in absorptance over entire spectrum**

the lower absorption coefficient of  $\mu\text{c-Si:H}$  caused by its indirect band gap [32]. In the below-band gap range, unlike for untreated a-Si:H, the absorptance curve for the treated film does not oscillate, because multiple reflections caused by the textured surface changes the transmitted light path through the film so that no rays will be reflected back to their original paths, eliminating the internal interference and oscillation.

In order to study the crystallization of the treated film, x-ray diffraction patterns were taken for both the untreated and treated a-Si:H films and are shown in Fig. 9 and 10. Both Figures show an amorphous peak around  $2\theta=25^\circ$ , which is caused by the internal constructive interference of the amorphous Si network. Two peaks at around  $2\theta=29^\circ$  and  $47^\circ$  emerge after processing which indicate a structural change after laser irradiation and can be indexed to the (111) and (220) crystalline orientations of silicon. As described in background section, an ultrafast non-thermally disorder-to-disorder phase transition occurs within a few picoseconds which cannot lead to crystallization. Then the material is partially melted due to the thermal diffusion after energy transfer from excited electrons to the material. The resolidification of the melted layer proceeds via vertical growth from the remaining unmelted material and results in random crystal orientations due to the amorphous structure of the film. According to the silicon powder diffraction file, the highest two intensities of x-ray diffraction are for the (111) and (220) orientations and are the same as observed in Fig. 10. The crystallization is considered to be under the partial melting regime, resulting in no preferential orientation during solidification. This suggests that the laser irradiated film becomes a mixture of  $\mu\text{c-Si:H}$  and a-Si:H with most of the  $\mu\text{c-Si:H}$  believed to be contained within the top melted surface.

### Further study of morphology

#### Effect of fluence and number of pulses

The surface morphology formation mechanism for crystalline silicon under laser processing has been described in background section. Further observation and understanding are

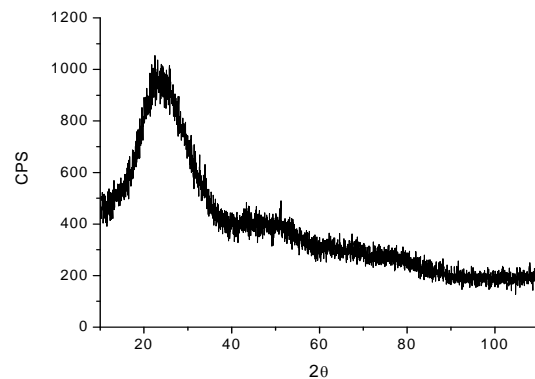


**Figure 9 XRD spectrum of as-received a-Si:H film, an “amorphous peak” around  $2\theta=25^\circ$  and no signs of crystallinity**

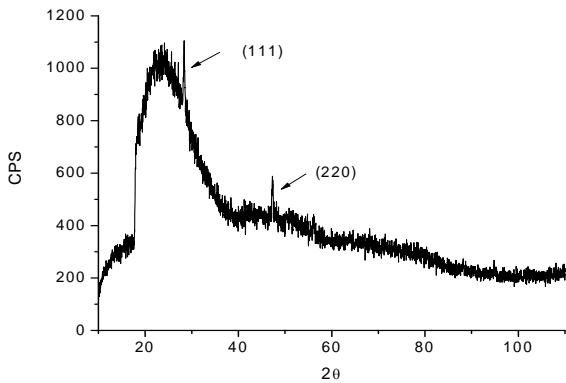


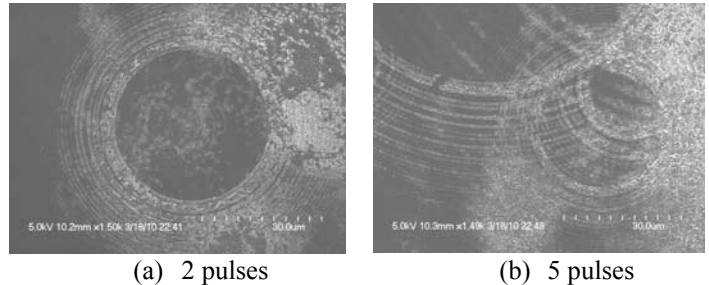
**Figure 10 XRD spectrum of laser treated a-Si:H film at fluence of  $0.5\text{J}/\text{cm}^2$  and scanning speed of  $25\text{ mm/s}$ , an “amorphous peak” around  $2\theta=25^\circ$ , existence of two overall different peaks for (111) and (220) orientation of silicon**

carried out. For his purpose, the sample is irradiated at a stationary point with various fluences ( $1\text{J}/\text{cm}^2$  to  $1.8\text{J}/\text{cm}^2$ ) and number of pulses (5 to 100).

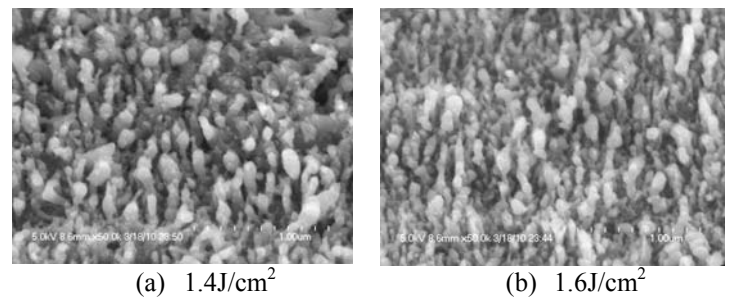
Figure 11 (a) and (b) show SEM images taken near the edges of the laser irradiated spot on an a-Si:H film surface after 2 and 5 pulses respectively with a fluence of  $1.4\text{J}/\text{cm}^2$ , and the spot diameter is  $150\text{ }\mu\text{m}$ . It can be seen that a ripple-like structure is generated on the surface after 2 pulses due to diffraction of the laser light by the micro-bubbles and that the spacing between the adjacent rings is closely matched to the laser wavelength ( $800\text{nm}$ ). After 5 pulses, at the edge of the irradiation area, it can be seen that ripples diffracted by separated bubbles start overlapping and generate a wavelength-dependent bead-like structure. When moving to the center of the area (not shown), the surface consisting of small spikes which are similar to those shown in Fig. 12 (a) suggests that more ripples are overlapping near the center of the beam, due to higher intensity in the center of the Gaussian beam that causes more decomposition of water and a greater number of bubbles to form. Figure 12 (a) and (b) show SEM images of the surface irradiated by 50 pulses at fluences of  $1.4\text{J}/\text{cm}^2$  and  $1.6\text{J}/\text{cm}^2$ , respectively. By 50 pulses, the entire irradiated area looks more uniform and the ripples have disappeared. Instead, nano-sized spikes are distributed on the surface which look more regular than those shown in Fig. 7. The reason is that the laser pulse is far beyond the ablation threshold so that all the material is ablated rather than melted and solidified. Interestingly, the spikes look quite similar at different fluences.

In order to further understand the correlation between the spike formation and fluence, AFM images were taken at the center ( $5\times 5\text{ }\mu\text{m}^2$ ) of samples irradiated by different fluences and numbers of pulses, and then the average spike height and spacing are calculated. In order to obtain reasonable value for the imperfect periodical morphology, peak identification from the AFM data was performed by first applying a smoothing filter in order to eliminate the labeling of small height

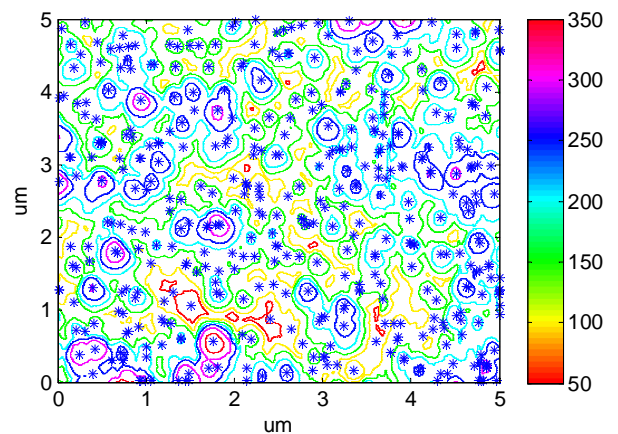
fluctuations as peaks. The peak positions were determined by finding points where the first order derivative is zero and second order derivative less than zero. A typical result is shown in Fig. 13, where stars indicate peak positions. The average distance to the 4 closest peaks is determined for each peak and the average spacing between the peaks can then be estimated.



**Figure 11 SEM images near the edge of laser irradiation area on a-Si:H film for (a) 2 pulses (b) 5 pulses at the fluence of  $1.4\text{J}/\text{cm}^2$ , the irradiation spot diameter is  $150\text{ }\mu\text{m}$ , showing superposition of diffraction fringes from separate bubbles**

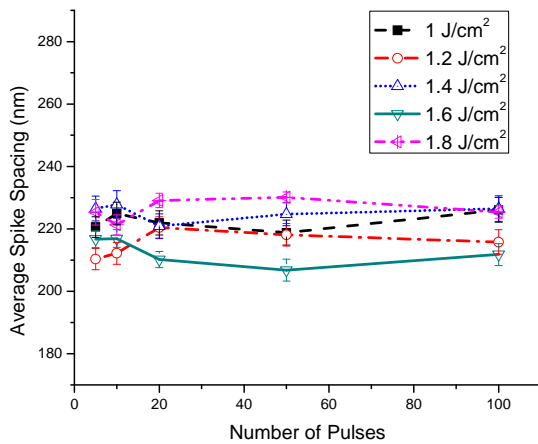


**Figure 12 SEM images of laser irradiation of a-Si:H film for 50 pulses at fluence of (a)  $1.4\text{J}/\text{cm}^2$  (b)  $1.6\text{J}/\text{cm}^2$ , the irradiation spot diameter is  $150\text{ }\mu\text{m}$ , showing similar spikes distributed on the surface**



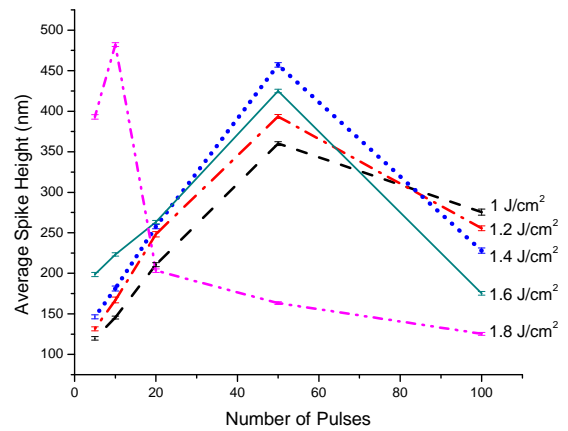
**Figure 13 Schematic of peak identification of extraction data from AFM images of laser irradiated a-Si:H film at different fluence and number of pulses, star means the identified peak point, solid curves indicate the contour spectra, AFM scanning area is  $5\times 5\text{ }\mu\text{m}$ , color bar unit: nm**

Figure 14 shows the average spike spacing is nearly constant for different fluences and number of pulses. Considering the imperfect spike distribution, this small variation range of 210-230 nm suggests that the separation between the spikes is stable at around 200 nm, and it is much smaller than that wavelength-dependent ripples formed at the beginning of irradiation. The similar phenomenon has been shown by Daminelli, et al. [21], the ripples generated on crystalline silicon with both wavelength-dependent and much thinner (~100 nm) spacing are observed after 100 pulses irradiation at a fluence of 1.5-1.6 J/cm<sup>2</sup>, and only 100 nm periodicity structures left after 1000 pulses. They suggested that this thinner spacing could be due to surface energy effects between the molten silicon and water which stabilizes more tightly spaced ripples. This may have some agreement that a-Si:H surface will be not stable after superposition of the wavelength-dependent ripples and further self-assembling process makes the surface stabilize at much smaller-spaced spikes. The larger spacing of 200 nm may be caused by different physico-chemical properties [33] between a-Si:H and crystalline silicon, which indicates that a-Si:H may have a larger surface energy during the processing so that the larger-spacing spikes are formed by a larger driving force. It is noted that, Shen, et al., [20] showed regular spikes with wavelength-dependent spacing that generated on a crystalline silicon surface by irradiating hundreds of pulses at a fluence of 0.76 J/cm<sup>2</sup>. This shows the surface can be stable after superposition of different diffracted ripples so that the self-assembling process will not occur. It may suggest that the self-assembling process have a “threshold”, if at a fluence lower than the “threshold”, the smaller-spaced surface structure will not be formed. However, for a-Si:H, this “threshold” may be lower than that of crystalline silicon, since at 0.5 J/cm<sup>2</sup>, the average spacing of spikes already becomes around 200 nm.



**Figure 14 Dependence of average spike spacing on fluence and number of pulses, error bars indicate standard error, the average spike height keeps constant at different conditions**

In Fig. 15, it can be seen that for the fluences of 1J/cm<sup>2</sup>, 1.2J/cm<sup>2</sup> and 1.4J/cm<sup>2</sup>, the average spike heights linearly increase with increasing fluence and number of pulses up to about 50 pulses. Due to the bead-like structure concentrating the light and causing the ablation rate beside the beads to be higher than that on the tips, the spikes are formed increasingly higher. After a few tens of pulses, the average height goes to a maximum which means that material between the spikes has been completely removed, therefore, the subsequent laser pulses start reducing the height of the spikes because the pulses only remove the material at the tips and the energy is not high enough to damage the substrate. This causes the average height of spikes after 100 pulses to be lower than that at 50 pulses. The tallest spikes after 100 pulses are formed for the lowest fluence of 1J/cm<sup>2</sup> since the ablation rate is proportional to fluence, resulting in the least spike tip ablation. At the higher fluences of 1.6 J/cm<sup>2</sup> and 1.8 J/cm<sup>2</sup>, the average peak heights follow the same overall trend with number of pulses as the lower fluences. However, the spike height after 50 pulses at 1.6 J/cm<sup>2</sup> is less than when processed at 1.4J/cm<sup>2</sup>, which means the spike height starts reducing by 50 pulses at 1.6 J/cm<sup>2</sup>. For an even higher fluence of 1.8 J/cm<sup>2</sup>, the point at which full-film-depth ablation occurs is after only 10 pulses, and the significantly reduction in peak height after 20 pulses indicates that nearly the whole film has been removed. The reason why the substrate between the spikes cannot be clearly seen in Fig. 12 (b) may be due to the re-deposition of ablated material. However, if the sample is irradiated by hundreds of pulses, it will be clear that the film has been fully removed at the center of the area (not shown).



**Figure 15 Dependence of average spike height on fluence and number of pulses, error bars indicate standard error**

Effect on absorption

To determine the optical absorption dependence on the surface morphology, the transmittance and reflectance of irradiated areas with different fluences and number of pulses are measured. The conditions are 1.2 J/cm<sup>2</sup> with 50 pulses and 1.4 J/cm<sup>2</sup> with 20 pulses, which generate average spike heights

of 393nm and 257nm, respectively. The scanning speed,  $v$ , is set by the FWHM of the Gaussian beam profile,  $d$ , the number of pulses,  $N$ , and the repetition rate of the laser,  $f$ , through the relation  $v=df/N$  [34]. No crystallinity was found in these two treated samples as estimated by XRD (not shown). Absorptance versus wavelength curves for both treated samples are shown in Fig. 16, and the absorptance results in Fig. 8 are also included for comparison. As described by Hua, et al. [35], the density, top angle and shape of the surface structure are the most important factors for absorption. Based on the constant spacing and similar shape of the generated spikes, these three factors are very similar for the three conditions investigated, therefore, for wavelengths with photon energies above the a-Si:H band gap ( $<730$  nm), the absorptance spectra of all laser treated samples are almost the same, no matter how deep the spikes are. The change in crystallinity is not significant here since the majority of the material is still a-Si:H after processing. The highest absorptance from the band gap to around 1600nm is for the sample processed at  $0.5\text{J}/\text{cm}^2$ , followed by  $1.4\text{J}/\text{cm}^2$  and  $1.2\text{J}/\text{cm}^2$  which suggests that the absorptance is inversely proportional to the spike height. This is because the below-band gap absorption is mainly dependent of the defect and impurity concentration in the a-Si:H layer and the multiple reflections due to surface texturing. Since the treated samples have similar multi-reflection abilities due to their similar surface geometries, and the sample treated at  $0.5\text{J}/\text{cm}^2$  has the smallest spikes and the thickest a-Si:H film underneath the textured layer, the highest absorptance occurs for a fluence of  $0.5\text{J}/\text{cm}^2$ . Moreover, the sample treated at  $0.5\text{J}/\text{cm}^2$  has a crystallized layer with a band gap of 1.1 eV, which helps to absorb light with wavelengths smaller than 1100nm. The reason that the trend reverses (compared with the curve trend in the range of 730nm to 1600nm) for wavelengths above 1600nm is not well understood at this point. However, based on the solar radiation spectrum, the radiation intensity in this range is a very small portion of the total intensity [28], which suggests that a lower absorption at these higher wavelengths will only have a small effect on the total energy absorption. Therefore, over the whole range of the spectrum, it can be concluded that the sample irradiated at  $0.5\text{J}/\text{cm}^2$  has the best absorption performance due to the combination of both surface texturing and crystallization.

## CONCLUSION

In conclusion, it has been demonstrated that improving the absorptance of sunlight and stability of a-Si:H thin films is possible through femtosecond laser irradiation in water. Absorptance enhancement is caused by light trapping based on the surface geometry, defects and impurity concentrations caused by the processing. The changes in crystallinity after processing reduces the thickness of the a-Si:H layer but may allow for greater stability in a-Si:H-based solar cells. Also, the crystallized material broadens the absorptance range to 1100nm. Furthermore, the formation of spikes on laser irradiated sample surfaces shows that the average spike spacing

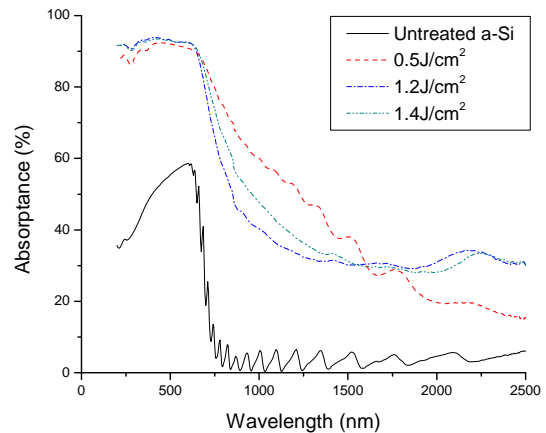


**Figure 16 Comparison of absorptance spectra measured by spectrophotometer of as-received and laser irradiated a-Si:H film at different fluence and pulse overlap ( $0.5\text{J}/\text{cm}^2$  at  $25\text{mm}/\text{s}$ ,  $1.2\text{J}/\text{cm}^2$  at 50 pulses,  $1.4\text{J}/\text{cm}^2$  at 20 pulses), showing enhanced absorptance for all processed samples**

is almost constant ( $\sim 200\text{nm}$ ) with different fluences and number of pulses. This has been suggested to be caused by the presence of water that influences the interface and the stabilization of much tightly spaced ripples. The average spike height is linearly increased by the laser fluence and number of pulses before the material between the spikes is completely removed, and then, an opposite trend is observed. Finally, the absorptance spectra indicate that the sample with both surface texturing and crystallization has the best absorption performance over the solar radiation spectrum, which suggests that femtosecond laser processing may allow for more efficient and economic a-Si:H thin film solar cell applications.

## ACKNOWLEDGMENTS

The use of material characteristic equipments at the Center for Functional Nanomaterials, Brookhaven National Laboratory and at Materials Research Science and Engineering Center, Columbia University is gratefully acknowledged.

## REFERENCES

- [1] Luque, A., Hegedus, S., 2003, "Handbook of Photovoltaic Science and Engineering", Wiley, UK, Chap. 7-8
- [2] Chopra, K.L., Paulson, P.D., Dutta, V., 2004, "Thin-Film Solar Cells: An Overview", Prog. Photovolt: Res. Appl. **12**, pp. 69-92
- [3] Kazmerski, L.L., 2006, "Solar Photovoltaics R&D at the Tipping Point: A 2005 Technology Overview", Journal of Electron Spectroscopy and related Phenomena, **150**, pp. 105-135
- [4] Miles, R.W., Hynes, K.M., Forbes, I., 2005, "Photovoltaic Solar Cells: An Overview of State-of-the-art Cell Development and Environmental Issues", Progress in Crystal Growth and Characterization of Materials, **51**, pp. 1-42

- [5] Staebler, D.L., Wronski, C.R., 1980, "Optically Induced Conductivity Changes in Discharge-produced Hydrogenated Amorphous Silicon", *Journals of Appl. Physics*, **51**(6)
- [6] Kolodziej, A., 2004, "Staebler-Wronski effect in amorphous silicon and its alloys", *Opto-electronics review*, **12**(1), pp. 21-32
- [7] Martirosyan, Kh.S., Hovhannisyan, A.S., Arouiounian, V.M., 2007, "Calculation of Reflectance of Porous Silicon Double-layer Antireflection Coating for Silicon Solar Cells", *Physica Status Solid (c)*, **4**(6), pp. 2103-2106
- [8] Hylton, J.D., Burgers A.R., Sinke, W.C., 2004, "Alkaline Etching for Reflectance Reduction in Multicrystalline Silicon Solar Cells", *J. of the Electro. Society*, **151**(6), pp. G408-G427
- [9] Fauchet, H.G., Siegman, A.E., 1982, "Surface ripples on silicon and gallium arsenide under picosecond laser illumination", *Appl. Phys. Lett.* **40**, pp. 824-826
- [10] Crouch, C.H., Carey, J.E., Warrender, J.M., Aziz, M.J., Mazur, E., Genin, F.Y., 2004, "Comparison of structure and properties of femtosecond and nanosecond laser-structured silicon", *Applied Physics Letters*, **84**(11), pp. 1850-1852
- [11] Yamamoto, K., et al., 2004, "A High Efficiency Thin Film Silicon Solar Cell and Module", *Solar Energy*, **77**, pp. 939-949
- [12] Gosain, D.P., Machida, A., Fujino, T., Hitsuda, Y., Nakano, K., Sato, J., 2003, "Formation of (100)-Textured Si Film Using an Excimer Laser on a Glass Substrate", *Jpn. J. Appl. Phys.*, **42**, pp. L135-L137
- [13] Shieh, J., Chen, Z., Dai, B., 2004, "Near-infrared Femtosecond Laser-induced Crystallization of Amorphous Silicon", *Applied physics letters*, **85**(7), pp. 1232-1234
- [14] Choi, T.Y., Hwang, D.J., Grigoropoulos, C.P., 2003, "Ultrafast laser-induced crystallization of amorphous silicon films", *Opt. Eng.*, **42**(11), pp. 3383-3388
- [15] Zheng, H.Y., Jiang, Z.W., 2010, "Femtosecond Laser Micromachining of Silicon with an External Electric Field", *Journal of Micromechanics and Microengineering*, **20**, 017001
- [16] Jiang, L., Tsai, H.L., 2003, "Femtosecond Laser Ablation: Challenges and Opportunities", *Proceeding of NSF Workshop on Research Needs in Thermal, Aspects of Material Removal*, Stillwater, OK, pp. 163-177
- [17] Tull, B.R., Carey, J.E., Mazur, E., McDonald, J.P., Yalisove, S.M., 2006, "Silicon Surface Morphologies after Femtosecond Laser Irradiation", *MRS Bulletin*, **31**(8), pp. 626-633
- [18] Sheehy, M.A., Winston, L., Carey, J.E., Friend, C.M., Mazur, E., 2005, "Role of the Background Gas in the Morphology and Optical Properties of Laser-Microstructured Silicon", *Chem. Mater*, **17**, pp. 3582-3586
- [19] Carey, J.E., 2004, "Femtosecond-laser Microstructuring of Silicon for Novel Optoelectronic Devices", Ph.D dissertation, Harvard University
- [20] Shen, M.Y., Crouch, C.H., Carey, J.E., Mazur, E., 2004, "Femtosecond Laser-induced Formation of Submicrometer Spikes on Silicon in Water", *Applied Physics Letters*, **85**(23), pp. 5694-5696
- [21] Daminelli, G., Kruger, J., Kautek, W., 2004, "Femtosecond Laser Interaction with Silicon Under Water Confinement", *Thin Solid Films*, **467**, pp. 334-341
- [22] Nayak, B.K., Gupta, M.C., 2007, "Femtosecond-laser-induced-crystallization and Simultaneous Formation of Light Trapping Microstructures in Thin a-Si:H Films", *Appl. Phys. A*, **89**, pp. 663-666
- [23] Gattass, R., Mazur, E., 2008, "Femtosecond Laser Micromachining in Transparent Materials", *Nature Photonics*, **2**, pp. 219-225
- [24] Sundaram, S.K., Mazur, E., 2002, "Inducing and Probing Non-thermal Transitions in Semiconductors Using Femtosecond Laser Pulses", *Nature Mat.*, **1**(4), pp. 217-224
- [25] Van Vechten, J.A., Tsu, R., Saris, F.W., 1979, "Nonthermal Pulsed Laser Annealing of Si; Plasma Annealing", *Physics Letters A*, **74**(6), pp. 422-426
- [26] Linde, D., Fabricius, N., 1982, "Observation of an Electronic Plasma in Picosecond Laser Annealing of Silicon", *Applied Physics Letter*, **41**(10), pp. 991-993
- [27] Callan, J.P., Kim, A., Roeser, C.A.D., Mazur, E., Solis, J., Siegel, J., Afonso, C.N., 2001, "Ultrafast Laser-induced Phase Transitions in Amorphous GeSb Films", *Physical Review Letters*, **86**(16), pp. 3650-3653
- [28] Goetzberger, A., Knobloch, J., Voss, B., 1998, "Crystalline Silicon Solar Cells", Wiley, Chichester, Chap. 2
- [29] Swanepoel, R., 1983, "Determination of the Thickness and Optical Constants of Amorphous Silicon", *J. Phys. E: Sci. Instrum.*, **16**, pp.1214-1222
- [30] Shaaban, E.R., 2008, "Calculation of Optical Constant of Amorphous Germanium Arsenoselenide Wedge-shaped Thin Films from Their Shrunk Transmittance and Reflectance Spectra", *Philosophical Magazine*, **88**(5), pp. 781-794
- [31] Kruger, J., Kautek, W., 1995, "Femtosecond-pulse Laser Processing of Metallic and Semiconducting Thin Films", *SPIE*, **2403**, pp. 436-447
- [32] Meillaud, F., et al., 2009, "Limiting Factors in the Fabrication of Microcrystalline Silicon Solar Cells and Microcrystalline/Amorphous ('Micromorph') Tandems", *Philosophical Magazine*, **89**(28), pp. 2599-2621
- [33] Kautek, W., Rudolph, P., Daminelli, G., Kriger, J., 2005, "Physico-chemical Aspects of Femtosecond-pulse-laser-induced Surface nanostructures", *Appl. Phys. A*, **81**, pp. 65-70
- [34] Crouch, C.H., Carey, J.E., Shen, M., Mazur, E., Fenin, F.Y., 2004, "Infrared Absorption by Sulfur-doped Silicon Formed by Femtosecond Laser Irradiation", *Applied Physics A*, **79**, pp. 1635-1641
- [35] Hua, X., Zhang, Y., Wang, H., 2010, "The Effect of Texture Unit Shape on Silicon Surface on the Absorption Properties", *Solar Energy Materials & Solar Cells*, **94**, pp. 258-262